



# Enhancement of Small-scale Turbulent Dynamo by Large-scale Shear

Nishant K. Singh<sup>1,2</sup> , Igor Rogachevskii<sup>2,3</sup> , and Axel Brandenburg<sup>2,4,5,6</sup> 

<sup>1</sup> Max-Planck-Institut für Sonnensystemforschung, Justus-von-Liebig-Weg 3, D-37077 Göttingen, Germany; [singh@mps.mpg.de](mailto:singh@mps.mpg.de)

<sup>2</sup> Nordita, KTH Royal Institute of Technology and Stockholm University, Roslagstullsbacken 23, SE-10691 Stockholm, Sweden; [brandenb@nordita.org](mailto:brandenb@nordita.org)

<sup>3</sup> Department of Mechanical Engineering, Ben-Gurion University of the Negev, P.O. Box 653, Beer-Sheva 84105, Israel; [gary@bgu.ac.il](mailto:gary@bgu.ac.il)

<sup>4</sup> JILA and Department of Astrophysical and Planetary Sciences, University of Colorado, Boulder, CO 80303, USA

<sup>5</sup> Department of Astronomy, AlbaNova University Center, Stockholm University, SE-10691 Stockholm, Sweden

<sup>6</sup> Laboratory for Atmospheric and Space Physics, University of Colorado, Boulder, CO 80303, USA

Received 2017 August 13; revised 2017 October 24; accepted 2017 October 25; published 2017 November 15

## Abstract

Small-scale dynamos (SSDs) are ubiquitous in a broad range of turbulent flows with large-scale shear, ranging from solar and galactic magnetism to accretion disks, cosmology, and structure formation. Using high-resolution direct numerical simulations, we show that in non-helically forced turbulence with zero mean magnetic field, large-scale shear supports SSD action, i.e., the dynamo growth rate increases with shear and shear enhances or even produces turbulence, which, in turn, further increases the growth rate. When the production rates of turbulent kinetic energy due to shear and forcing are comparable, we find scalings for the growth rate  $\gamma$  of the SSD and the turbulent rms velocity  $u_{\text{rms}}$  with shear rate  $S$  that are independent of the magnetic Prandtl number:  $\gamma \propto |S|$  and  $u_{\text{rms}} \propto |S|^{2/3}$ . For large fluid and magnetic Reynolds numbers,  $\gamma$ , normalized by its shear-free value, depends only on shear. Having compensated for shear-induced effects on turbulent velocity, we find that the normalized growth rate of the SSD exhibits the scaling,  $\tilde{\gamma} \propto |S|^{2/3}$ , arising solely from the induction equation for a given velocity field.

*Key words:* dynamo – magnetic fields – magnetohydrodynamics (MHD) – turbulence

## 1. Introduction

In an electrically conducting turbulent fluid, the dynamo is a fundamental phenomenon that can explain the origin of magnetic fields in solar-like stars, galaxies, accretion disks, etc. Two types of turbulent dynamos are usually discussed in the literature: large-scale and small-scale dynamos (SSDs; see, e.g., Moffatt 1978; Zeldovich et al. 1990; Brandenburg & Subramanian 2005). Magnetic field generation on scales smaller and larger than the integral scale of turbulence are described as SSD and large-scale dynamo (LSD), respectively. The SSDs are ubiquitous and naturally find applications in a broad range of topics such as galactic magnetism (Kulsrud & Anderson 1992; Rieder & Teyssier 2016), solar coronal heating (Amari et al. 2015), accretion disks (Blackman & Nauman 2015), cosmology and structure formation (Pakmor et al. 2014; Soker 2017), Riemannian manifolds (Sokoloff & Rubashny 2013), formation of the first stars in the Universe (Schleicher et al. 2010), etc.

The nature of the SSD depends strongly on the magnetic Prandtl number,  $\text{Pr}_M = \nu/\eta$  (see, e.g., Kulsrud & Anderson 1992; Haugen et al. 2004; Schekochihin et al. 2004, 2005; Brandenburg 2011), where  $\eta$  is the magnetic diffusivity due to the electrical conductivity of the plasma and  $\nu$  is its kinematic viscosity. Random stretching of the magnetic field by smooth velocity fluctuations in the viscous subrange of scales describes the SSD for  $\text{Pr}_M \gg 1$  (see, e.g., Zeldovich et al. 1990; Kleeorin & Rogachevskii 1994; Subramanian 1998; Kleeorin et al. 2002; Haugen et al. 2004; Schekochihin et al. 2004, 2005; Bhat & Subramanian 2014). The SSD at low  $\text{Pr}_M$  is excited by the turbulent inertial-range velocity fluctuations (the spatially rough velocity field). The growth rate of the SSD at low  $\text{Pr}_M$  is determined by the resistive magnetic diffusion scale (see, e.g., Kazantsev 1968; Vainshtein & Zeldovich 1972; Rogachevskii & Kleeorin 1997; Boldyrev & Cattaneo 2004; Isakov et al. 2007;

Schekochihin et al. 2007; Kleeorin & Rogachevskii 2012; Schober et al. 2012).

Large-scale velocity shear is a common feature of many astrophysical flows in, e.g., solar and stellar convective zones, galaxies, and accretion disks (see, e.g., Moffatt 1978; Zeldovich et al. 1990; Brandenburg & Subramanian 2005). In recent years, a non-helical turbulent shear dynamo has been discussed, where the presence of large-scale shear in turbulence with zero mean kinetic helicity yields an LSD (see, e.g., Sokoloff 1997; Vishniac & Brandenburg 1997; Rogachevskii & Kleeorin 2003; Brandenburg 2005; Brandenburg et al. 2008; Käpylä et al. 2008; Kleeorin & Rogachevskii 2008; Yousef et al. 2008; Sridhar & Subramanian 2009; Sridhar & Singh 2010, 2014; Singh & Sridhar 2011). The main conclusion from these studies is that a combination of homogeneous non-helical turbulence and large-scale shear is able to generate a large-scale magnetic field without any mean kinetic helicity. Like many other large-scale turbulent dynamos, they yield pronounced large-scale magnetic structures. Large-scale shear in non-helical turbulence also causes a “vorticity dynamo,” i.e., the excitation of a large-scale instability, resulting in an exponential growth of the mean vorticity (Elperin et al. 2003; Yousef et al. 2008; Käpylä et al. 2009).

In turbulence with large-scale shear, the SSD can be strongly affected by shear, notably because turbulence itself can be produced by the shear. However, the details related to the effect of shear on the SSD are unclear. A recent analytical study by Kolokolov et al. (2011) has demonstrated that, for a given random smooth velocity field, large-scale shear can support an SSD such that the dynamo growth rate, which we denote by  $\tilde{\gamma}$  arising solely from the induction equation, increases with shear rate  $S$  as  $\tilde{\gamma} \propto |S|^{2/3}$ . This is compatible with an upper bound for growth rates discussed in Proctor (2012).

In this Letter, we study the effects of large-scale shear on an SSD using high-resolution direct numerical simulations (DNS)

for different magnetic Prandtl numbers ranging from 0.5 to 10. To avoid interference from other effects, we consider shear as the only source of non-isotropy and thus neglect gravity. We ignore turbulent heating effects, which would lead to undesired secular changes of the background state. We also ignore related refinements such as a polytropic instead of an isothermal equation of state, which causes only negligible differences (Brandenburg & Kahnishvili 2017). We make the shearing box approximation, so there is no feedback on the imposed large-scale velocity shear.

Using the budget equation for turbulent kinetic energy, we develop a framework for identifying a scaling function that we then determine in DNS. In agreement with earlier work by Kolokolov et al. (2011), we demonstrate that the growth rate of an SSD in non-helically forced turbulence increases with the shear rate.

## 2. Budget Equation

Because large-scale shear can affect the turbulent velocity, we start with a theoretical analysis based on the budget equation for turbulent kinetic energy,  $\mathcal{E}_K = \frac{1}{2}\overline{\mathbf{u}^2}$ , assuming incompressibility (Monin & Yaglom 1971):

$$\frac{D\mathcal{E}_K}{Dt} + \text{div } \Phi_K = -\overline{u_i u_j} \nabla_j \overline{U}_i + \overline{\mathbf{u} \cdot \mathbf{f}_f} - \varepsilon, \quad (1)$$

where  $D/Dt = \partial/\partial t + \overline{\mathbf{U}} \cdot \nabla$  is the advective derivative,  $\mathbf{u}$  is the fluctuating velocity,  $\overline{\mathbf{U}}$  is the mean velocity, and  $\varepsilon$  is the dissipation rate of  $\mathcal{E}_K$ . The term  $\Phi_K = \rho^{-1}\overline{\mathbf{u}p} + \overline{\mathbf{u}u^2}/2$  includes the third-order moments that determine the flux of  $\mathcal{E}_K$ , where  $p$  are the pressure fluctuations, and  $\rho$  is the fluid density. The term  $\overline{\mathbf{u} \cdot \mathbf{f}_f}$  in Equation (1) describes the production rate of turbulence caused by external forcing, while the first term in the right-hand side of Equation (1) determines the turbulence production rate caused by large-scale shear.

The Reynolds stresses in isotropic turbulence (Monin & Yaglom 1971; Elperin et al. 2002) are

$$\overline{u_i u_j} = \frac{\overline{u^2}}{3} \delta_{ij} - \frac{\nu_T}{2} (\nabla_i \overline{U}_j + \nabla_j \overline{U}_i), \quad (2)$$

where  $\nu_T$  is the turbulent viscosity and  $\delta_{ij}$  is the Kronecker tensor. For the sake of simplicity, let us consider turbulence with a linear velocity shear,  $\overline{\mathbf{U}} = (0, Sx, 0)$ , which results in anisotropy of turbulence. However, the modification of the Reynolds stresses by anisotropic turbulence does not change the turbulence production rate caused by linear velocity shear; see Equation (A33) and (12) in Elperin et al. (2002). The dissipation rate of  $\mathcal{E}_K$  for large fluid Reynolds numbers is estimated as  $\varepsilon \sim \mathcal{E}_K/\tau_f = u_{\text{rms}}^3/2\ell_f$  (Monin & Yaglom 1971), while the turbulent viscosity is estimated as  $\nu_T \sim \ell_f u_{\text{rms}}/3$ , where  $\ell_f$  is the integral scale of the turbulence,  $u_{\text{rms}} = \sqrt{\overline{\mathbf{u}^2}}$ , and  $\tau_f = \ell_f/u_{\text{rms}}$  is the characteristic turbulent time based on the integral scale.

Substituting Equation (2) into Equation (1) we obtain

$$\frac{D\mathcal{E}_K}{Dt} + \text{div } \Phi_K = \overline{\mathbf{u} \cdot \mathbf{f}_f} + \frac{\nu_T}{2} S^2 - \frac{u_{\text{rms}}^3}{2\ell_f}. \quad (3)$$

Depending on the value of shear, Equation (3) implies the following scalings for  $u_{\text{rms}}(S)$  in stationary homogeneous turbulence.

(i) *Small shear*: the turbulent production rate caused by the forcing is much larger than that caused by the shear, so that  $u_0^3/2\ell_f \sim \overline{\mathbf{u} \cdot \mathbf{f}_f}$ , and  $\nu_T = \nu_T^{(0)} \sim \ell_f u_0/3$ , where  $u_0 = u_{\text{rms}}(S=0)$ . For small shear,  $u_{\text{rms}}$  is weakly dependent on shear.

(ii) *Intermediate shear*: the turbulent production rates caused by the forcing and the shear are of the same order, and the balance,  $u_{\text{rms}}^3/\ell_f \sim \nu_T^{(0)} S^2$ , yields the following scaling:  $u_{\text{rms}} \propto |S|^{2/3}$ .

(iii) *Strong shear*: the turbulent production rate in Equation (3) caused by the forcing can be neglected, so that turbulence is produced only by shear. The steady-state solution of the equation,  $\nu_T S^2 - u_{\text{rms}}^3/\ell_f = 0$ , yields the scaling  $u_{\text{rms}} = S \ell_f$ . This implies that for shear-produced turbulence, the small-scale shear rate  $u_{\text{rms}}/\ell_f$  cannot be much smaller than the large-scale shear.

## 3. Growth Rate of the SSD

Let us consider first the case  $\text{Pr}_M \ll 1$ , when the resistive magnetic diffusion scale is much larger than the Kolmogorov viscous scale. This implies that the resistive scale is located inside the inertial range of the turbulence, where the fluid motions are spatially rough. The SSD occurs due to random stretching of the magnetic field by the turbulent velocity, while scale-dependent turbulent magnetic diffusivity causes dissipation of the magnetic field. At the resistive scale, the scale-dependent turbulent magnetic diffusivity approaches  $\eta$ . The strongest magnetic field stretching is at small scales, i.e., at the resistive scale. Therefore, the growth rate of the SSD (far from the threshold) in turbulence without large-scale shear for  $\text{Pr}_M \ll 1$  is estimated as the inverse resistive time (see, e.g., Kazantsev 1968; Schekochihin et al. 2007):

$$\gamma_0 \sim u_\eta/\ell_\eta \sim \tau_f^{-1} \text{Re}_M^{1/2}, \quad (4)$$

where  $u_\eta = (\varepsilon \ell_\eta)^{1/3}$  is the characteristic turbulent velocity at the resistive scale,  $\ell_\eta$ , and  $\text{Re}_M$  is the magnetic Reynolds number.

Using Equation (4), we assume that the growth rate of the SSD instability with large-scale shear, normalized by that without shear, can be estimated as

$$\frac{\gamma(S)}{\gamma_0} \sim \left( \frac{u_{\text{rms}}(S)}{u_0} \right)^{1/2} \tilde{\gamma}(S), \quad (5)$$

where  $\gamma_0 = \gamma(S=0)$  and  $u_0 = u_{\text{rms}}(S=0)$  represent the dynamo growth rate and the rms velocity for  $S=0$ , and  $\tilde{\gamma}(S=0) = 1$ . Let us define the normalized rms velocity,  $\tilde{u}_{\text{rms}} = u_{\text{rms}}(S)/u_0$ . Here we assumed that the turbulent forcing scale,  $\ell_f$ , is independent of large-scale shear. The contribution  $\tilde{u}_{\text{rms}}^{1/2}$  to the dynamo growth rate is caused by the effect of large-scale shear on the turbulent velocity field, while the function  $\tilde{\gamma}(S)$  determines the effect of large-scale shear on the growth of the SSD instability for a given turbulent velocity field. Thus the normalized growth rate,  $\tilde{\gamma}$ , which can be interpreted as a contribution to the dynamo growth rate arising solely from the induction equation for a given velocity field, can be expressed as

$$\tilde{\gamma} = \gamma(S)/(\gamma_0 \sqrt{\tilde{u}_{\text{rms}}}). \quad (6)$$

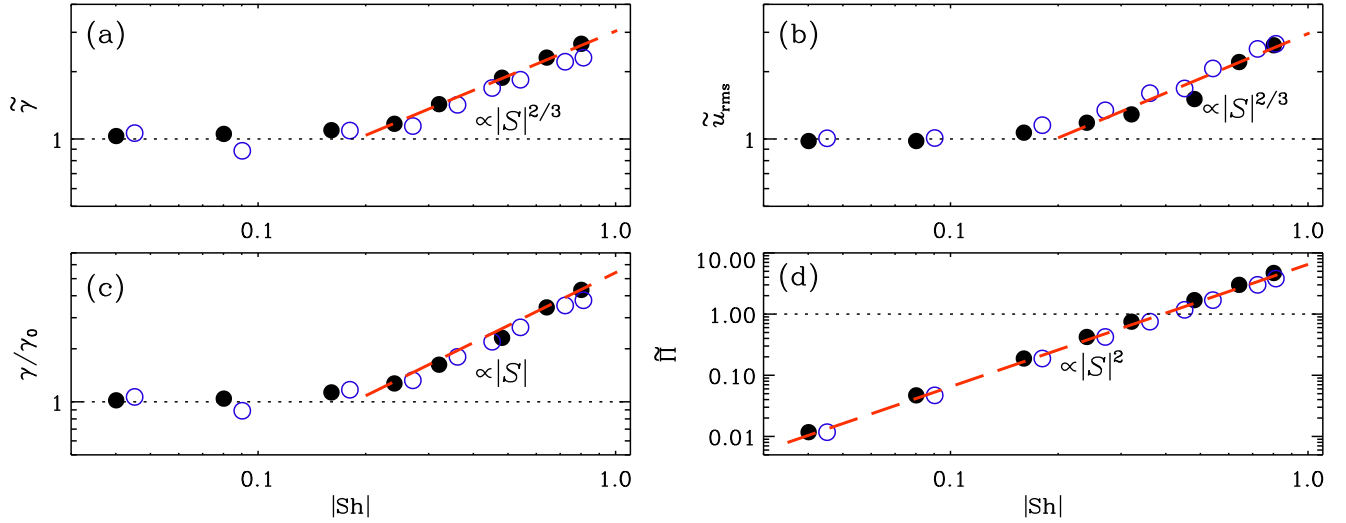


**Figure 1.** Shear dependencies of (a)  $\tilde{\gamma}$ , (b)  $\tilde{u}_{rms}$ , (c)  $\gamma/\gamma_0$ , and (d)  $\tilde{\Pi}$ , shown for two choices of  $\text{Pr}_M$ , both sets having  $u_{max}/c_s = 0.07$ , and  $|S|_{max}/c_s k_f = 0.02$ . Filled (black) circles:  $\text{Pr}_M = 0.5$  with  $\gamma_0/u_0 k_f = 0.02$ , and  $\text{Re}_M^{(0)} \equiv u_0/k_f \eta = 121$ ; open (blue) circles:  $\text{Pr}_M = 3$ , with  $\gamma_0/u_0 k_f = 0.05$ , and  $\text{Re}_M^{(0)} \equiv u_0/k_f \eta = 148$ .

It is useful to define the ratio of the turbulent production rates caused by shear and forcing,

$$\tilde{\Pi} = \frac{\Pi_S}{\Pi_f} = \frac{\nu_r S^2}{u_{rms} f} = \frac{2\pi S^2}{3k_f f}. \quad (7)$$

For  $\text{Pr}_M \gg 1$ , magnetic fluctuations are determined by the smooth velocity field in the viscous subrange. We assume that in turbulence with large-scale shear, Equation (5) is also valid for  $\text{Pr}_M \geq 1$ . In the next section we perform DNS to determine the scaling laws for  $\gamma(S)/\gamma_0$  and  $u_{rms}(S)/u_0$ .

#### 4. Numerical Setup

We consider low-Mach-number compressible isothermal magnetohydrodynamic turbulence with background shear,  $\bar{\mathbf{U}}^S = (0, Sx, 0)$  with  $S < 0$ , and a white-noise non-helical random statistically homogeneous isotropic body force  $\mathbf{f}$  as the source of turbulent motions. The departure  $\mathbf{U}$  from the mean shear flow obeys

$$\frac{D\mathbf{U}}{Dt} = -\mathbf{U} \cdot \nabla \mathbf{U} + S U_x \hat{\mathbf{y}} - c_s^2 \nabla \ln \rho + \rho^{-1} \mathbf{J} \times \mathbf{B} + \mathbf{f} + \mathbf{F}_{visc}, \quad (8)$$

$$\frac{D \ln \rho}{Dt} = -\mathbf{U} \cdot \nabla \ln \rho - \nabla \cdot \mathbf{U}, \quad (9)$$

$$\frac{D\mathbf{A}}{Dt} = -S A_y \hat{\mathbf{x}} + \mathbf{U} \times \mathbf{B} - \eta \mathbf{J}, \quad (10)$$

where  $D/Dt \equiv \partial_t + Sx \nabla_y$  is the advective derivative with respect to  $\bar{\mathbf{U}}^S$ ,  $\mathbf{B} = \nabla \times \mathbf{A}$  is the magnetic field in terms of the vector potential  $\mathbf{A}$ ,  $\mathbf{F}_{visc} = \rho^{-1} \nabla \cdot (2\nu \rho \mathbf{S})$  is the viscous force,  $\mathbf{S}_{ij} = \frac{1}{2}(\nabla_i U_j + \nabla_j U_i) - \frac{1}{3} \delta_{ij} \nabla \cdot \mathbf{U}$  is the traceless rate of strain tensor,  $\mathbf{J} = \nabla \times \mathbf{B}/\mu_0$  is the current density,  $\mu_0$  is the vacuum permeability, and  $c_s$  is the isothermal sound speed. These equations are solved with shearing-periodic boundary conditions using the PENCIL CODE (<https://github.com/pencil-code>). It uses sixth-order explicit finite differences in space and a third-order accurate time-stepping method.

We solve Equations (8)–(10) in a cubic domain of size  $L^3$  using  $512^3$  or  $1024^3$  spatial resolution and choose  $k_f = 2.2 k_1$ , where  $k_1 = 2\pi/L$ . Thus the chosen stochastic forcing injects energy at scales close to the box scale. This allows us to study the SSD in the absence of the LSD, or the so-called shear dynamo, that is also expected to be excited in such a setup. However, the LSD would require a reasonably large scale separation. Nevertheless, the growth rates measured from an early kinematic stage predominantly reflect the growth of the SSD, which grows at a rate much faster than that of the possible LSD.

The system of equations is characterized by the following set of non-dimensional numbers:

$$\begin{aligned} \text{Re}_M &= \frac{u_{rms}}{\eta k_f}, & \text{Re} &= \frac{u_{rms}}{\nu k_f}, & \text{Pr}_M &= \frac{\nu}{\eta}, \\ \text{Sh} &= \frac{S}{u_0 k_f}, & \tilde{\text{Sh}} &= \frac{S}{u_{rms} k_f}, & \Sigma_f &= \frac{c_s \nu k_1^2}{f} \end{aligned} \quad (11)$$

where  $\text{Re}$  and  $\text{Re}_M$  are the fluid and magnetic Reynolds numbers,  $\text{Pr}_M$  is the magnetic Prandtl number,  $\text{Sh}$  and  $\tilde{\text{Sh}}$  are the shear parameters based on  $u_0$  and  $u_{rms}$ , respectively, and  $\Sigma_f$  characterizes the inverse forcing.

#### 5. DNS Results

In this section we discuss the results of DNS and compare them with the theoretical predictions.

##### 5.1. The Dynamo Growth Rate and Production of Turbulence

First we determine the SSD growth rate as a function of  $S$ . To this end we drop the Lorentz force in the momentum Equation (8). In Figure 1 we show the shear dependencies of (i) the normalized dynamo growth rate,  $\tilde{\gamma}(S)$  which is defined by Equation (6), (ii) the normalized rms velocity,  $\tilde{u}_{rms} = u_{rms}(S)/u_0$ , (iii) total growth rate  $\gamma$ , and (iv) the ratio of turbulence production rates  $\tilde{\Pi}$ , for two values of  $\text{Pr}_M$  (smaller and larger than unity). Figure 1 demonstrates the existence of the following scalings for intermediate shear when the ratio  $\tilde{\Pi}$

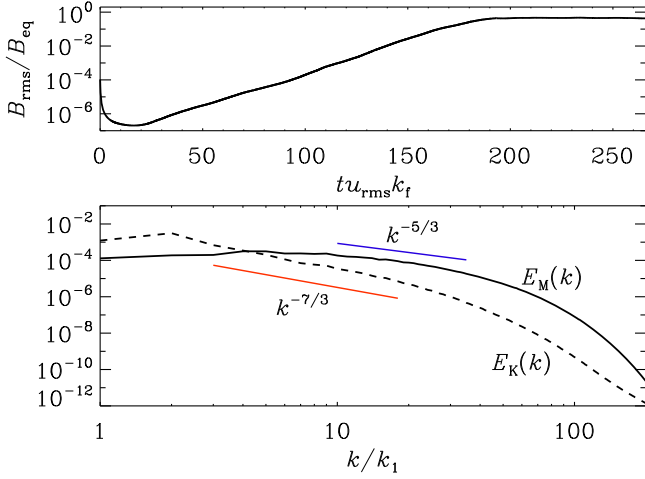


**Figure 2.** Nonlinear evolution of  $B_{\text{rms}}/B_{\text{eq}}$  (upper panel) and spectra of magnetic  $E_M(k)$  (solid curve) and kinetic  $E_K(k)$  (dashed curve) energies in the saturation stage (lower panel) at  $\text{Pr}_M = 10$  with  $|\tilde{\text{Sh}}| = 0.23$ ,  $u_{\text{rms}}/c_s = 0.04$  and  $|S|/c_s k_f = 0.009$ .

is of the order of unity:

$$\gamma/\gamma_0 \propto |S|, \quad \tilde{u}_{\text{rms}} \propto |S|^{2/3}, \quad \tilde{\gamma} \propto |S|^{2/3}. \quad (12)$$

These scalings are independent of  $\text{Pr}_M$ . The SSD growth rate increases with shear, which implies that large-scale shear supports the SSD. The obtained DNS scaling for  $\tilde{\gamma}$  coincides with that found by Kolokolov et al. (2011) from the solution of the equation for the pair correlation function of the magnetic field. This equation was derived from the induction equation for a given random smooth velocity field.

### 5.2. Nonlinear Stage of the SSD

In Figure 2 we plot the nonlinear evolution of  $B_{\text{rms}}/B_{\text{eq}}$  and spectra of magnetic,  $E_M(k)$ , and kinetic,  $E_K(k)$ , energies in the saturation stage, where  $B_{\text{eq}} = (\mu_0 \rho)^{1/2} u_{\text{rms}}$  is the equipartition magnetic field. Magnetic fluctuations reach saturation at the equipartition level and have a short inertial range compatible with a  $k^{-5/3}$  spectrum. At larger scales, the velocity is compatible with a  $k^{-7/3}$  spectrum, which is expected for anisotropic sheared fluctuations produced by tangling of the large-scale gradient of the mean velocity by the background random velocity field. This spectrum was predicted analytically by Lumley (1967), detected in atmospheric turbulence by Wyngaard & Cote (1972), and confirmed in DNS by Ishihara et al. (2002).

Figure 3 shows results based on  $1024^3$  simulations at  $\text{Pr}_M = 10$  for varying forcing strengths while keeping the shear rate  $S$  as fixed. The turbulence is produced by shear in all three cases, which yields the same  $u_{\text{rms}}$  in the saturated state, thus resulting in the same value for the shear parameter  $\tilde{\text{Sh}}$ . The growth rates of SSD are found to be identical, as would be expected from our above findings. Note that the onset of the dynamo growth is delayed for weaker forcing (e.g., the red curve in Figure 3).

### 5.3. Mean Flow Generation

Figure 2 demonstrates the fact that shear fundamentally modifies the nature of background turbulence, resulting in a  $k^{-7/3}$  spectrum, which leads to the generation of a large-scale flow. In Figure 4 we show a spacetime diagram of the mean

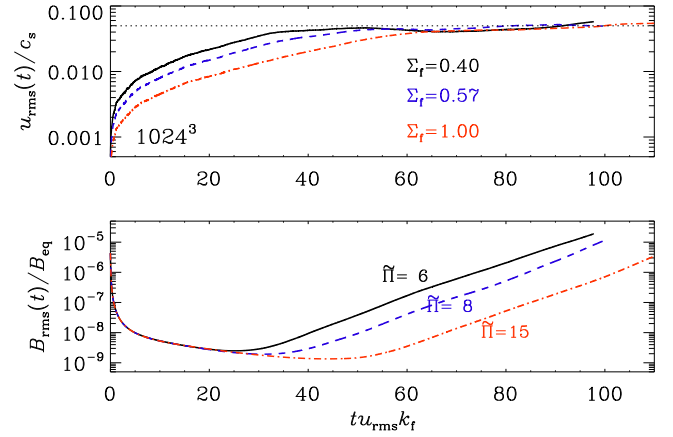


**Figure 3.** Temporal evolution of  $u_{\text{rms}}$  and  $B_{\text{rms}}$  from three runs with solid, dashed, and dashed-dotted curves in the order of decreased forcing, while all other parameters are the same:  $\text{Pr}_M = 10$ ,  $\text{Re} = 220$ ,  $|\tilde{\text{Sh}}| = 0.3$ ,  $u_{\text{rms}}/c_s = 0.05$ , and  $|S|/c_s k_f = 0.02$ . For all three cases, we find  $\gamma/u_{\text{rms}}k_f = 0.146$ .

flow components,  $\bar{U}_x$  and  $\bar{U}_y$ , where the mean is obtained by applying a planar (here  $xy$ ) average. Both  $\bar{U}_x$  and  $\bar{U}_y$  spontaneously develop a mean pattern in the direction normal to the shear plane. Such a generation of mean flow was first explored by Elperin et al. (2003), and numerically demonstrated by Yousef et al. (2008) and Käpylä et al. (2009). The mean flow pattern begins to develop after a few tens of eddy turnover time,  $(u_{\text{rms}}k_f)^{-1}$ . We found that  $\bar{U}_y$  is about four times stronger compared to  $\bar{U}_x$  and both are excited in phase, which is in agreement with Käpylä et al. (2009).

### 5.4. Saturation of the Shear Parameter

Based on  $512^3$  simulations at magnetic Prandtl number  $\text{Pr}_M = 0.5$  and 3, we showed in Figure 1(b) that the  $u_{\text{rms}}$  increases with shear. The dimensionless shear parameter,  $\tilde{\text{Sh}}$ , defined with respect to  $u_{\text{rms}}(S)$ , is thus expected to approach saturation at large shear rates in the regime of shear-produced turbulence. Here we check the saturation of  $\tilde{\text{Sh}}$  by performing a suite of lower resolution,  $128^3$ , simulations at  $\text{Pr}_M = 1$ . For a fixed shear rate, we explore the shear-produced turbulence regime (i.e., the regime with  $\tilde{\Pi} > 1$ ) by successively decreasing the forcing strength, i.e., by increasing  $\Sigma_f$ ; see Equations (7) and (11) for definitions of  $\tilde{\Pi}$  and  $\Sigma_f$ , respectively.

In Figure 5, we demonstrate the saturation of the shear parameter,  $\tilde{\text{Sh}}$ , as a function of  $\Sigma_f$ . Two different choices of the shear rate result in the overlap of  $1/|\tilde{\text{Sh}}|$  at large values of  $\Sigma_f$  and show saturation at a constant level corresponding to  $|\tilde{\text{Sh}}| \approx 3/4\pi$ . Thus, in a realistic setup with subsonic turbulence, such as the one being studied here, it would not be possible to explore values of  $|\tilde{\text{Sh}}|$  that are much larger than about 0.25. Note that the abscissae in Figure 1 correspond to  $\text{Sh}$ , which is defined with respect to  $u_0$ , instead of  $u_{\text{rms}}(S)$ , and therefore extend up to about unity.

The effect of shear on the SSD becomes noticeable only when shear rate exceeds a certain threshold such that the turbulence production ratio,  $\tilde{\Pi}$ , becomes of order unity or larger. This results in a narrow range of possible values for the shear parameter in order to determine the scalings of the SSD growth rates versus shear rate. Thus, one interesting regime of a very strong shear is not found in DNS.

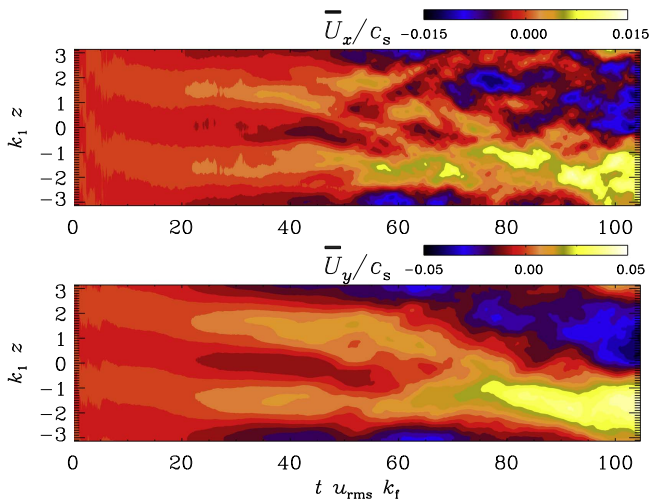


**Figure 4.**  $\bar{U}_x$  (top) and  $\bar{U}_y$  (bottom) as functions of time and  $z$  from a  $1024^3$  simulation with  $\text{Pr}_M = 10$ ,  $|\tilde{S}h| = 0.3$ ,  $\tilde{\Pi} = 15$  and  $u_{\text{rms}}/c_s = 0.046$ .

## 6. Discussion

It is worth noting that recent simulations by Tobias & Cattaneo (2013) of a prescribed deterministic non-helical flow with large-scale shear and a superposition of small-scale cellular deterministic flows have shown that large-scale shear reduces the SSD growth rate. In those simulations, the Navier–Stokes equation is not used, so the effects of shear-produced turbulence, whereby large-scale shear increases the turbulent velocity, have been ignored. As a result, shear suppresses the SSD by a sweeping effect, i.e., the shear decorrelates the small eddies from the magnetic field by advecting the field. On the other hand, in our study a different setup is used, where large-scale shear fundamentally modifies and even produces turbulence, and enhances the efficiency of the SSD. Notably, the generation of non-uniform mean velocity field, as shown in Figure 4, was not observed in Tobias & Cattaneo (2013). This additionally confirms the difference between their setup and ours.

Remarkably, we obtain from DNS the same scaling,  $\tilde{\gamma}(S) \propto |S|^{2/3}$ , for SSD growth rate as was theoretically predicted by Kolokolov et al. (2011) for a given velocity field. Interestingly, the occurrence of intermittent shear bursts was found to increase the growth rate of the SSD in turbulent magnetoconvection (Pratt et al. 2013).

In the present study we considered isothermal non-stratified low-Mach number turbulence, where the main contribution to the SSD comes from small resistive or viscous scales. At these scales, all of the anisotropic effects caused by gravity are negligibly small. Earlier numerical simulations performed for turbulent convection without imposed large-scale shear have shown that the properties of the SSD (growth rates and characteristic magnetic scales) are similar to those for forced isothermal turbulence; see, e.g., the review by Brandenburg & Subramanian (2005). We can expect that the inclusion of large-scale shear does not introduce strong differences for the SSD in turbulence with and without gravity.

In turbulence with imposed shear, a large-scale magnetic field can be generated by an LSD with a much smaller growth rate than for the SSD. The generated SSD can affect the growing large-scale magnetic field, but in the present Letter we have not studied the LSD and its interaction with the SSD. In particular, by applying periodic or shearing-periodic boundary

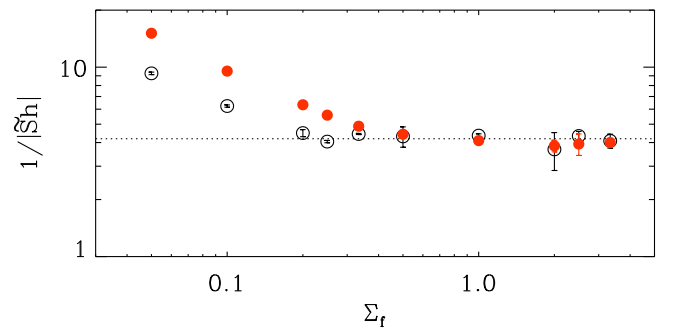


**Figure 5.** Saturation of the shear parameter  $\tilde{S}h$  as a function of  $\Sigma_f$  for two choices of shear rate,  $|S|/c_s k_f = 0.022$  (black open circles) and  $|S|/c_s k_f = 0.013$  (red filled circles), both at  $\text{Pr}_M = 1$ . Larger values of  $\Sigma_f$  correspond to the regime where the turbulence is predominantly produced by shear. The dotted line represents  $|\tilde{S}h| = 3/4\pi$ .

conditions, and by injecting energy through our forcing at the box scale, LSD effects such as the incoherent  $\alpha$ -shear effect (Sokoloff 1997; Vishniac & Brandenburg 1997; Sridhar & Singh 2014) and  $\eta$  quenching (caused by the feedback of the large-scale magnetic field on the turbulence; Guerrero et al. 2009) are suppressed. Note also that global-scale magnetic fields can produce small-scale magnetic fields by tangling. However, this growth of the magnetic field is linear in time rather than exponential. These effects could develop stronger gradients and thus perhaps islands of different orientation, but those would not systematically affect the SSD.

## 7. Conclusions

Using DNS, it was demonstrated that the SSD growth rate increases with shear in non-helical turbulence. The scalings for the growth rate of the SSD,  $\gamma \propto |S|$ , and for the turbulent velocity,  $u_{\text{rms}} \propto |S|^{2/3}$ , are independent of  $\text{Pr}_M$ , when the turbulent production rates caused by shear and forcing are of the same order. The contribution to the dynamo growth rate,  $\tilde{\gamma} \propto |S|^{2/3}$ , is also found to be independent of  $\text{Pr}_M$ . This contribution is determined solely by the equation for the pair correlation function of the magnetic field derived from the induction equation.

We found that large-scale shear has the following three different effects that are relevant for turbulent SSD:

1. the direct effect of shear on the generation of small-scale magnetic fields through the induction equation;
2. the production of turbulence by the shear which further enhances the SSD action; and
3. the generation of large-scale non-uniform motions due to interaction of turbulence with mean shear by the vorticity dynamo, which in turn produces new large-scale shear, thus enhancing the SSD.

We have benefited from stimulating discussions with Pallavi Bhat, Nathan Kleeorin, Igor Kolokolov, Dhruvadya Mitra, Matthias Rheinhardt, Kandaswamy Subramanian, and Steve Tobias. I.R. thanks NORDITA for hospitality and support during his visits. This work has been supported in parts by the NSF Astronomy and Astrophysics Grants Program (grant 1615100), the Swedish Research Council grant No. 621-2011-5076, and the Research Council of Norway under the FRINATEK grant No. 231444. We acknowledge the allocation of computing resources provided by the Swedish National

Allocations Committee at the Center for Parallel Computers at the Royal Institute of Technology in Stockholm, and by CSC—IT Center for Science Ltd. in Espoo, Finland, which is administered by the Finnish Ministry of Education (project 2000403).

### ORCID iDs

Nishant K. Singh  <https://orcid.org/0000-0001-6097-688X>  
 Igor Rogachevskii  <https://orcid.org/0000-0001-7308-4768>  
 Axel Brandenburg  <https://orcid.org/0000-0002-7304-021X>

### References

- Amari, T., Luciani, J., & Aly, J. 2015, *Natur*, **522**, 188  
 Bhat, P., & Subramanian, K. 2014, *ApJ*, **791**, L34  
 Blackman, E. G., & Nauman, F. 2015, *JPIPh*, **81**, 395810505  
 Boldyrev, S., & Cattaneo, F. 2004, *PhRvL*, **92**, 144501  
 Brandenburg, A. 2005, *ApJ*, **625**, 539  
 Brandenburg, A. 2011, *ApJ*, **741**, 92  
 Brandenburg, A., & Kahniashvili, T. 2017, *PhRvL*, **118**, 055102  
 Brandenburg, A., Rädler, K.-H., Rheinhardt, M., & Käpylä, P. J. 2008, *ApJ*, **676**, 740  
 Brandenburg, A., & Subramanian, K. 2005, *PhR*, **417**, 1  
 Elperin, T., Kleeorin, N., & Rogachevskii, I. 2003, *PhRvE*, **68**, 016311  
 Elperin, T., Kleeorin, N., Rogachevskii, I., & Zilitinkevich, S. S. 2002, *PhRvE*, **66**, 066305  
 Guerrero, G., Dikpati, M., & de Gouveia Dal Pino, E. M. 2009, *ApJ*, **701**, 725  
 Haugen, N. E. L., Brandenburg, A., & Dobler, W. 2004, *PhRvE*, **70**, 016308  
 Ishihara, T., Yoshida, K., & Kaneda, Y. 2002, *PhRvL*, **88**, 154501  
 Iskakov, A. B., Schekochihin, A. A., Cowley, S. C., McWilliams, J. C., & Proctor, M. R. E. 2007, *PhRvL*, **98**, 208510  
 Käpylä, P. J., Korpi, M. J., & Brandenburg, A. 2008, *A&A*, **491**, 353  
 Käpylä, P. J., Mitra, D., & Brandenburg, A. 2009, *PhRvE*, **79**, 016302  
 Kazantsev, A. P. 1968, *JETP*, **26**, 1031  
 Kleeorin, N., & Rogachevskii, I. 1994, *PhRvE*, **50**, 493  
 Kleeorin, N., & Rogachevskii, I. 2008, *PhRvE*, **77**, 036307  
 Kleeorin, N., & Rogachevskii, I. 2012, *PhyS*, **86**, 018404  
 Kleeorin, N., Rogachevskii, I., & Sokoloff, D. 2002, *PhRvE*, **65**, 036303  
 Kolokolov, I. V., Lebedev, V. V., & Sizov, G. A. 2011, *JETP*, **113**, 339  
 Kulsrud, R. M., & Anderson, S. W. 1992, *ApJ*, **396**, 606  
 Lumley, J. L. 1967, *PhFl*, **10**, 1405  
 Moffatt, H. K. 1978, *Magnetic Field Generation in Electrically Conducting Fluids* (New York: Cambridge Univ. Press)  
 Monin, A. S., & Yaglom, A. M. 1971, *Statistical Fluid Mechanics*, Vol. 1 (Cambridge, MA: MIT Press)  
 Pakmor, R., Marinacci, F., & Springel, V. 2014, *ApJ*, **783**, L20  
 Pratt, J., Busse, A., & Müller, W.-C. 2013, *A&A*, **557**, A76  
 Proctor, M. R. E. 2012, *JFM*, **697**, 504  
 Rieder, M., & Teysier, R. 2016, *MNRAS*, **457**, 1722  
 Rogachevskii, I., & Kleeorin, N. 1997, *PhRvE*, **56**, 417  
 Rogachevskii, I., & Kleeorin, N. 2003, *PhRvE*, **68**, 036301  
 Schekochihin, A. A., Cowley, S. C., Taylor, S. F., Maron, J. L., & McWilliams, J. C. 2004, *ApJ*, **612**, 276  
 Schekochihin, A. A., Haugen, N. E. L., Brandenburg, A., et al. 2005, *ApJ*, **625**, L115  
 Schekochihin, A. A., Iskakov, A. B., Cowley, S. C., et al. 2007, *NJPh*, **9**, 300  
 Schleicher, D. R. G., Banerjee, R., Sur, S., et al. 2010, *A&A*, **522**, A115  
 Schober, J., Schleicher, D., Federrath, Ch., Klessen, R., & Banerjee, R. 2012, *PhRvE*, **85**, 026303  
 Singh, N. K., & Sridhar, S. 2011, *PhRvE*, **83**, 056309  
 Soker, N. 2017, *MNRAS*, **466**, 4776  
 Sokoloff, D., & Rubashny, A. 2013, *GApFD*, **107**, 403  
 Sokoloff, D. D. 1997, *ARep*, **41**, 68  
 Sridhar, S., & Singh, N. K. 2010, *JFM*, **664**, 265  
 Sridhar, S., & Singh, N. K. 2014, *MNRAS*, **445**, 3770  
 Sridhar, S., & Subramanian, K. 2009, *PhRvE*, **80**, 066315  
 Subramanian, K. 1998, *MNRAS*, **294**, 718  
 Tobias, S. M., & Cattaneo, F. 2013, *Natur*, **497**, 463  
 Vainshtein, S. I., & Zeldovich, Ya. B. 1972, *SvPhU*, **15**, 159  
 Vishniac, E. T., & Brandenburg, A. 1997, *ApJ*, **475**, 263  
 Wyngaard, J. C., & Cote, O. R. 1972, *QJRM*, **98**, 590  
 Yousef, T. A., Heinemann, T., Schekochihin, A. A., et al. 2008, *PhRvL*, **100**, 184501  
 Zeldovich, Ya. B., Ruzmaikin, A. A., & Sokoloff, D. D. 1990, *The Almighty Chance* (London: Word Scientific)